

## Evaluation of tree growth relevant atmospheric circulation patterns for geopotential height field reconstructions for Asia

**Andrea Seim, Johannes A. Schultz, Christoph Beck, Achim Bräuning, Paul J. Krusic, Caroline Leland, Oyunsanaa Byambasuren, Eryuan Liang, Xiaochun Wang, Jee-Hoon Jeong, Hans W. Linderholm**

### Angaben zur Veröffentlichung / Publication details:

Seim, Andrea, Johannes A. Schultz, Christoph Beck, Achim Bräuning, Paul J. Krusic, Caroline Leland, Oyunsanaa Byambasuren, et al. 2018. "Evaluation of tree growth relevant atmospheric circulation patterns for geopotential height field reconstructions for Asia." *Journal of Climate* 31 (11): 4391-401.  
<https://doi.org/10.1175/jcli-d-17-0164.1>.

### Nutzungsbedingungen / Terms of use:

Dieses Dokument wird unter folgenden Bedingungen zur Verfügung gestellt: / This document is made available under the following conditions:

**Sonstige Open-Access-Lizenz**

Weitere Informationen finden Sie unter: / For more information see:  
[https://www.bibliothek.uni-augsburg.de/opus/lic\\_sonst.html](https://www.bibliothek.uni-augsburg.de/opus/lic_sonst.html)

licsonst



## 🔗 Evaluation of Tree Growth Relevant Atmospheric Circulation Patterns for Geopotential Height Field Reconstructions for Asia

ANDREA SEIM,<sup>a,b</sup> JOHANNES A. SCHULTZ,<sup>c</sup> CHRISTOPH BECK,<sup>d</sup> ACHIM BRÄUNING,<sup>e</sup>  
PAUL J. KRUSIC,<sup>f,g,h</sup> CAROLINE LELAND,<sup>i</sup> OYUNSANAA BYAMBASUREN,<sup>j</sup>  
ERYUAN LIANG,<sup>k</sup> XIAOCHUN WANG,<sup>l</sup> JEE-HOON JEONG,<sup>m</sup> AND  
HANS W. LINDERHOLM<sup>a</sup>

<sup>a</sup> Regional Climate Group, Department of Earth Sciences, University of Gothenburg, Gothenburg, Sweden

<sup>b</sup> Institute for Forest Growth IWW, University of Freiburg, Freiburg, Germany

<sup>c</sup> Geomatics Research Group, Department of Geography, Ruhr-University Bochum, Bochum, Germany

<sup>d</sup> Institute of Geography, University of Augsburg, Augsburg, Germany

<sup>e</sup> Institute of Geography, Friedrich-Alexander Universität Erlangen-Nürnberg, Erlangen, Germany

<sup>f</sup> Navarino Environmental Observatory, Costa Navarino, Greece

<sup>g</sup> Department of Physical Geography, Stockholm University, Stockholm, Sweden

<sup>h</sup> Department of Geography, University of Cambridge, Cambridge, United Kingdom

<sup>i</sup> Tree Ring Laboratory, Lamont-Doherty Earth Observatory, Palisades, New York

<sup>j</sup> Regional Central Asia Fire Management Resource Center, National University of Mongolia, Ulaanbaatar, Mongolia

<sup>k</sup> Key Laboratory of Tibetan Environment Changes and Land Surface Processes, Institute of Tibetan Plateau Research, Chinese Academy of Sciences, Beijing, China

<sup>l</sup> Center for Ecological Research, Northeast Forestry University, Harbin, Heilongjiang, China

<sup>m</sup> Department of Oceanography, Chonnam National University, Gwangju, South Korea

(Manuscript received 14 March 2017, in final form 26 January 2018)

### ABSTRACT

Atmospheric circulations influence local and regional weather conditions and, thus, tree growth. To identify summer weather types relevant for tree growth, and their associated synoptic-scale circulation patterns, an atmospheric circulation tree ring index (ACTI) dataset, derived from 414 tree-ring sites across Asia spanning the period 1871–2010, was created. Modes of common variability in the ACTI dataset were compared with leading modes of observed summertime 500-hPa geopotential height. The first four ACTI modes (explaining 88% of the total variance) were associated with pressure centers over Eurasia, the tropics, and the Pacific Ocean. The high spatiotemporal resemblance between the leading circulation modes, derived from both tree rings and 500-hPa geopotential height fields, indicates a strong potential for reconstructing large-scale circulation patterns from tree rings in Asia. This would allow investigations of natural atmospheric circulation variability prior to anthropogenic climate change and provide a means to validate model simulations of climate predictions.

### 1. Introduction

Globally observed changes in land and ocean temperatures, glacier and polar ice extents, and extreme weather events, such as droughts or floods, during the

🔗 Denotes content that is immediately available upon publication as open access.

📎 Supplemental information related to this paper is available at the Journals Online website: <https://doi.org/10.1175/JCLI-D-17-0164.s1>.

Corresponding author: Andrea Seim, [andrea.seim@iww.uni-freiburg.de](mailto:andrea.seim@iww.uni-freiburg.de)

past century are indicators of anthropogenic climate change (IPCC 2013; Coumou and Rahmstorf 2012). In Asia, where the vast majority of the population depends on agricultural productivity, changes in local and regional climate conditions have severe consequences for societies and environments alike (Hansen and Cramer 2015; Mirza 2011; Rao et al. 2015). Local and regional weather or climate conditions are largely controlled by atmospheric circulation patterns (Barry and Perry 1973), including the distribution of pressure patterns and the occurrence and intensity of monsoons or jet streams. Yet, the dynamics and response of the atmosphere to climate change still pose a challenge for climate model

DOI: 10.1175/JCLI-D-17-0164.1

© 2018 American Meteorological Society. For information regarding reuse of this content and general copyright information, consult the AMS Copyright Policy ([www.ametsoc.org/PUBSReuseLicenses](http://www.ametsoc.org/PUBSReuseLicenses)).

simulations, as demonstrated by Shepherd (2014) for the Atlantic–European sector.

Paleo-proxy data provide useful information for climate model validations, especially annually resolved terrestrial proxies with wide geographical distributions, such as tree rings. In the extratropics, tree growth is influenced by local and regional weather conditions during the growing season of the current and previous years (Fritts 1976). Tree-ring width (TRW), latewood density, and stable isotope composition have been widely used for reconstructions of past temperature and hydroclimate variability in Asia on regional (e.g., Davi et al. 2015; Fang et al. 2010; Krusic et al. 2015; Liang et al. 2008; Sano et al. 2013; Solomina et al. 2014; Wernicke et al. 2017b; Yadav et al. 2011) and continental scales (Ahmed et al. 2013; Cook et al. 2010; Shi et al. 2015). Because of Asia's size and varying topography, its climate is diverse, especially during summer, when westerly winds as well as the Asian monsoons influence surface climates (Figs. 1 and 2). To gain a better understanding of atmospheric circulation patterns that influence past and present climates in Asia, previous studies using annual TRW variations have focused on temporal rather than spatial associations. Standard empirical methods to infer circulation patterns from tree rings generally involve correlation statistics (e.g., on extreme growth years) and spectral analyses, matching cyclic variations in tree growth or other wood parameters with atmospheric circulation indices, such as the North Atlantic Oscillation or El Niño–Southern Oscillation (e.g., Li et al. 2013; Linderholm et al. 2009; Michaelsen 1989). However, a comprehensive description of the complexity in the spatiotemporal interaction between surface climate and atmospheric circulation is not possible with those methods. A new method was introduced by Schultz and Neuwirth (2012) that directly links tree growth to synoptic-scale weather patterns in Europe by generating an atmospheric circulation tree ring index (ACTI). This method uses a Monte Carlo simulation to calculate the influence of each weather type on tree growth at a specific site. The procedure has proven to capture weather-type signals in tree-ring chronologies (Schultz et al. 2015) for regions with complex climate controls on tree growth, like mid-latitude Asia (Seim et al. 2016).

Here, we applied this new method to a multispecies, continental-scale network of 414 TRW chronologies located across Asia. We focused on the summer season [June–August (JJA)], where the majority of the tree-ring records show strong climate responses, and when the spatiotemporal climate and atmospheric circulation variability are most complex and not well understood. We investigated the associations between TRW and

atmospheric pressure anomalies to gain a better understanding of the circulation patterns controlling tree growth and their spatiotemporal characteristics at a continental scale. Results were compared to observed conditions.

## 2. Data and methods

### a. Tree-ring data

We compiled a network of 414 TRW chronologies from 12 countries within the domain 25°–60°N, 50°–165°E (Fig. 1a). The majority of the data were downloaded from the International Tree-Ring Data Bank (<http://www.ncdc.noaa.gov/paleo/treering.html>), and the remainder were provided by the authors (Table S1 in the supplemental material). The network is composed predominantly of chronologies from coniferous species (98.8% of all chronologies), that is, larch (*Larix* spp.), juniper (*Juniperus* spp.), spruce (*Picea* spp.), pine (*Pinus* spp.), and fir (*Abies* spp.), and five broadleaf species chronologies (birch, walnut, poplar, oak, and elm) (Fig. 1b). The elevation of the sites ranges from 10 m MSL (Skahalín Island, Russia) to 4480 m MSL (Nyinchi in the Tibetan Plateau, China). The distribution of the species is reflected by their tolerance to cold or dry environments and to certain edaphic (e.g., soil type and bedrock) conditions. For instance, larch, spruce, and pine are most common in the lowlands (e.g., in the boreal forests in Siberia, Russia), whereas fir, juniper, and spruce are dominant at higher elevations, such as in and around the Tibetan Plateau (Figs. 1a,c).

To study the climate information recorded in tree rings, a TRW chronology was developed for each of the 414 sites, with the aim to preserve the climate signal and remove any nonclimatic trends; for example, the distinct decreasing trend in raw ring width with the increasing biological age and diameter of a tree. This age trend was eliminated while preserving interannual-to-decadal variability in the tree-ring data by fitting a 32-yr cubic smoothing spline to each series (Cook and Peters 1981, 1997). Additionally, we improved each chronology by removing biases resulting from temporally uneven sample size by applying a power transformation (Cook and Peters 1997) to each raw TRW series prior to detrending, as well as variance stabilization (Osborn et al. 1997). Each TRW chronology was truncated at a minimum of five series to reduce biases caused by a low sample replication, subsequently leading to an overall common period of 1889–1978. The correlation values between all TRW series in a chronology and the common signal strength of the chronologies—that is, the expressed population signal (Wigley et al. 1984), a quality measure

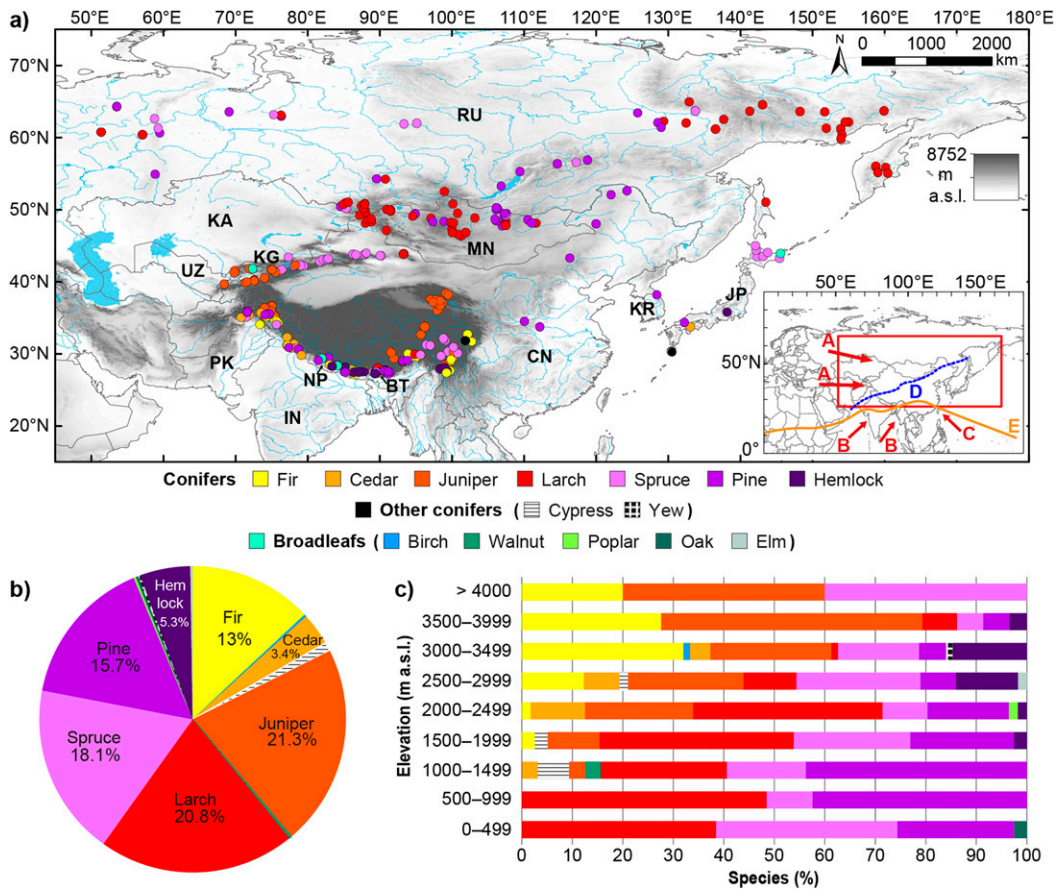


FIG. 1. (a) Spatial distribution of the tree-ring sites in the study area (red square in inset) with dominant climate influences during summer from the westerlies (A), Indian summer monsoon (B), East Asian summer monsoon (C) in the context of the modern monsoon limit (D) [after Chen et al. (2008) and Yancheva et al. (2007)], and the position of the intertropical convergence zone (E) and the spatial distribution of the 414 individual site chronologies (see legend for species). (b) Species composition of the tree-ring network and (c) with respect to elevation. Color and pattern assignment for each species is provided in the legend.

for each chronology—proved to be suitable for dendroclimatological analyses.

*b. Reanalysis data*

To study the behavior and movement of circulation patterns that persist over several days, mean pressure fields are grouped into distinctive classes (so-called large-scale weather or circulation types). Since subjective classifications do not exist for the whole of Asia, we applied an objective, statistically validated classification scheme. To do this, we used the NOAA–CIRES twentieth-century reanalysis data (Compo et al. 2011) for the summer season (June–August), available for the period 1871–2010. The 1000-, 850-, 700-, and 500-hPa geopotential height NOAA–CIRES data (hereafter, H1000, H850, H700, and H500, respectively) were run through the COST733 classification software (Philipp et al. 2016) to search for distinct

synoptic daily patterns on a 2° × 2° spatial grid resolution. Consideration is given to 1) the presence of several high mountain ranges (e.g., the Himalayas) and the Tibetan Plateau (mean elevation of ~4500 m MSL) and 2) the vertical extension of dominant atmospheric circulation patterns, like the Asian monsoons. The final classification for each geopotential height field was done using a cluster analysis based on the distributed *k*-means approach, since it best resolves surface climate variations (Enke and Spekat 1997). We produced a classification scheme of 27 predefined weather types, which occur over the course of a year within the region of 25°–65°N, 45°–165°E. This domain covers all the relevant circulation patterns of influence over Asia from the subtropical (below 25°N) to subpolar (above 65°N) regions. Those weather types prevailing only during the summer (June–August) were used for further analyses.

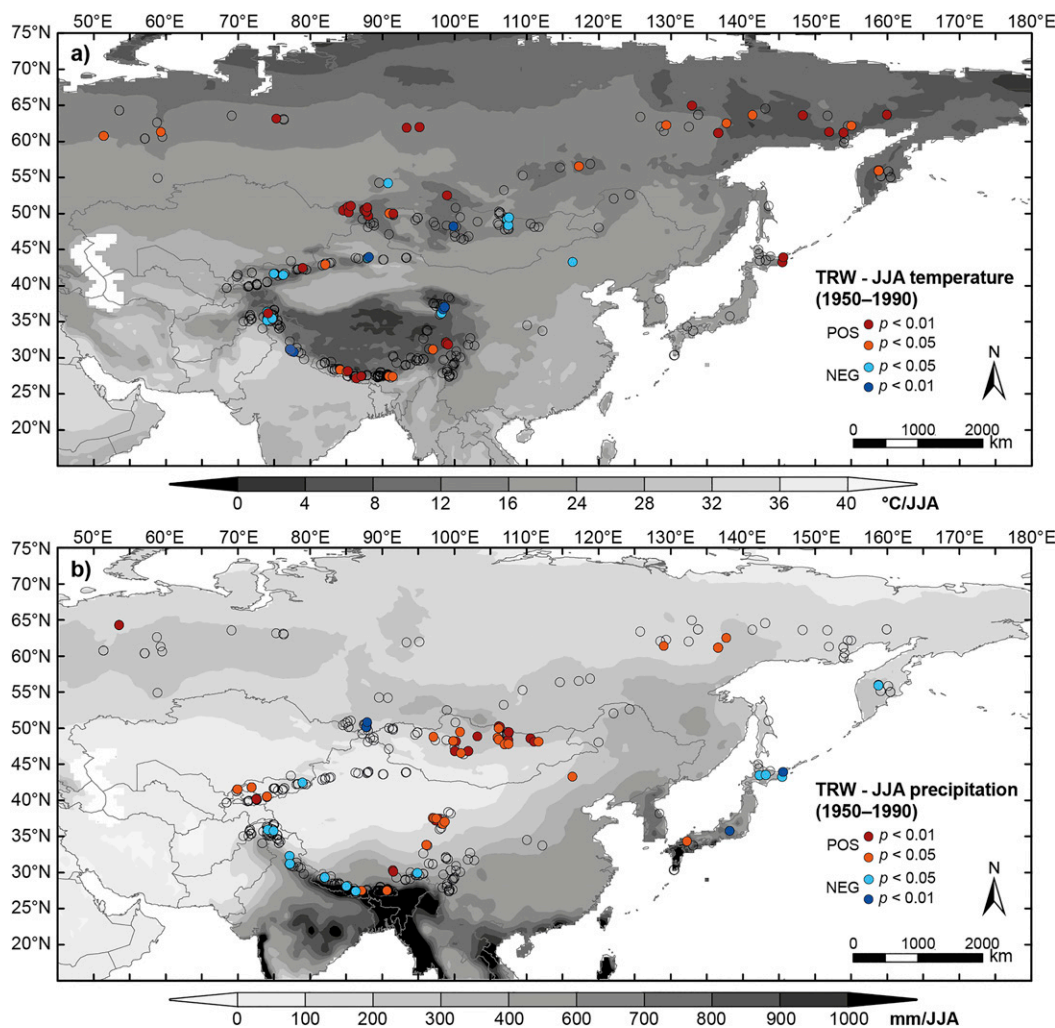


FIG. 2. Correlation statistics for all detrended 414 TRW chronologies with color-filled circles showing a significant JJA (a) temperature and (b) precipitation response over the period 1950–90. Significance levels (see legend) were adjusted regarding end dates of the individual chronologies, and gridpoint climate data from the CRU time series, version 3.23 (TS3.23), dataset were averaged for  $5^{\circ} \times 5^{\circ}$  subregions. Background gray-scale map shows JJA (a) mean of monthly temperature and (b) sum of monthly precipitation over the period 1950–90.

### c. Identification of tree-growth-relevant atmospheric circulation patterns during summer

To identify and extract individual tree-growth responses to the classified large-scale weather types, we subjected each TRW chronology to a new procedure to generate an ACTI record (Schultz and Neuwirth 2012). The ACTI time series are defined as June–August sums of the weighted weather-type frequencies during the period 1871–2010, expressed as

$$\text{ACTI}_y = \sum_{j=1}^w (h_{yj} \times g_j). \quad (1)$$

The prevailing weather types  $j = 1, \dots, w$  (different for each geopotential height), their frequency  $h_{yj}$ , and their

weight  $g_j$  are used to calculate  $\text{ACTI}_y$ , with  $y = 1, \dots, t$  (here,  $t = 140$ , for 1871–2010) for the summer season (1 June–31 August).

The aim of the ACTI procedure is to identify and extract tree-growth-relevant climate drivers that are better explained by weather types than by temperature and precipitation. Therefore, the calculation of the ACTI is slightly more complex. While the frequency of each weather type  $h_{yj}$  is simply the number of days (between June and August) of its occurrence, a statistical model is needed to calculate the influence ( $g_j$ ) that each weather type has on tree growth at a site to produce the ACTI. The following procedure is repeated for all four geopotential heights:

- 1) The calculation of  $10^6$  randomly weighted weather-type indices using a Monte Carlo simulation with

- 10<sup>6</sup> random number sets. Thus, a matrix with normal distributed random numbers (here, 1 000 000 multiplied by the number of summertime weather types) is generated.
- 2) Identification of those randomly weighted weather-type indices that have the strongest statistical relationships with the site chronologies using a five-stage selection procedure:
    - (i) the Pearson correlation over 60 discontinuous years between 1889 and 1978, to avoid overfitting of the model;
    - (ii) a sequential goodness-of-fit metatest (Carvajal-Rodriguez et al. 2009), for a multiple comparison adjustment;
    - (iii) Spearman rank correlation coefficients, to reduce the influence of outliers;
    - (iv) selection of best-performing weather-type indices and associated random number sets; and
    - (v) calculation of weather-type weights: averaging all associated random number sets for each chronology if more than 500 passed all selection criteria.

When a negative correlation is found between the chronology and weather-type indices, the corresponding random number sets were multiplied by  $-1$  before the averaging was performed.
  - 3) The calculation of the ACTI for each site chronology using the representative weather-type weights and Eq. (1).

The weights thus represent the influence of each weather type on tree growth at each site. For more elaborate explanations on the approach, see Seim et al. (2016, chapter 2.3) and Schultz and Neuwirth (2012). We calculated an ACTI time series covering the full 1871–2010 period for each of the four weather-type classifications (i.e., classification of the four isobaric surfaces) and for all TRW chronologies that showed a significant ( $p < 0.05$ ) summertime weather-type response. The resulting ACTI time series were standardized to a mean of zero and a variance of one.

It should be noted that not all sites showed a significant ( $p < 0.05$ ) response to the classified weather types at each of the four pressure levels. When there was more than one ACTI series calculated for one site (Table S1), we averaged all ACTI records for each site over the four isobaric surfaces (from H1000 to H500) and continued working with an ensemble mean, proven to yield more robust and statistically significant results (Schultz et al. 2015).

To describe common tree growth within the ensemble ACTI network, we applied a principal component analysis (PCA) (Peters et al. 1981) over the full 1871–2010 period. The principal components that explained

most of the common variability in the ensemble ACTI network were retained for further study. In addition, we conducted a PCA on June–August H500 pressure data from the NOAA–CIRES twentieth-century reanalysis dataset over the same region as for the weather-type classification (25°–65°N, 45°–165°E) and for the same time period (1871–2010). This was done to identify dominant observed atmospheric circulation patterns, which allows us to evaluate the resulting ACTI modes, that is, tree-growth-relevant circulation patterns, with the leading modes of the observed pressure at H500.

Spatial correlation maps between the leading ACTI principal components and different climate parameters (e.g., temperature, precipitation, and sea level pressure) were computed using the climate explorer (<http://climexp.knmi.nl/>) (Van Oldenborgh and Burgers 2005) over the shorter period 1901–2010. The resulting spatial correlation maps, computed for the ACTI principal components, were compared to spatial correlation patterns of the leading modes of the observed pressure at H500 and the same climate parameters.

### 3. Results and discussion

#### *a. Characteristics of the most frequent summertime weather types*

The number of objectively classified summertime weather types  $j$  for the different pressure heights ranged from a minimum of eight for H500 to a maximum of 20 for H850. From those, however, only a few occurred with a frequency of more than 10% (equals  $\sim 9$  days) of all summer days per year between 1871 and 2010 (Fig. S1 in the supplemental material). At H1000 (H850), a feature common to the five (four) most frequent weather types was a low pressure center over the southwestern parts of the study area ( $\sim 30^\circ\text{N}$ ,  $70^\circ\text{E}$ ), as indicated by low geopotential heights (Figs. S1a,b). Although this pattern slightly varied in intensity and location, the prevailing wind directions across the study area were from the north-northeast and southeast. Overall, this low pressure center represents the southwest Asian low, which dominates weather conditions during summer in Asia (Dando 2005). Using the NOAA–CIRES twentieth-century reanalysis data, the southwest Asian low was classified for 96.6% (77.5%) of all summer days at H1000 (H850), which corresponds to about 88 days (70.5 days) of the 92 summer days per year during 1871 and 2010. At higher levels (from H700 to H500), the dominant wind directions changed to northwest and west as a result of high pressure centers developed over central Asia and the Tibetan Plateau (Figs. S1c,d).

From the 414 TRW chronologies, significant ( $p < 0.05$ ) responses to summertime circulation patterns were found for 219 chronologies at H1000, 281 chronologies at H850, 190 chronologies at H700, and 147 chronologies at H500. Only 50 chronologies showed no significant response to pressure anomalies at any of the four isobaric surfaces; thus, no ACTI record was calculated (Table S1). However, chronologies with insignificant or weak weather-type responses contributed indirectly to the final results. After averaging all ACTI records for each site over all geopotential heights, the final ensemble ACTI dataset comprises 339 sites.

Using PCA, 12 ACTI modes were extracted (all with eigenvalues greater than one) that explained 99.2% of the network's variance. However, we only focused on the first four ACTI modes (from ACTI\_1 to ACTI\_4) that together explain 88.4% of the total variance.

### *b. Tree-growth-relevant synoptic-scale circulation patterns*

By definition, positive (negative) ACTI values denote high (low) tree-growth increments and hence, favorable (unfavorable) growing conditions for the trees. However, trees from different sites respond weaker or even contrary to the same large-scale weather pattern. For instance, at the H1000 height, TRW chronologies showed correlation values with temperature ranging from  $-0.4$  to  $0.68$  ( $p < 0.05$ ), and for precipitation sensitive chronologies, correlation values vary from  $-0.54$  to  $0.48$  ( $p < 0.05$ ). This is mainly related to different environmental controls on tree growth at the sites (Fritts 1976). Tree growth at high altitudes (i.e., upper tree line) and high latitudes is enhanced by warm temperatures, whereas tree growth at low-elevation sites and across midlatitude semiarid and arid areas is limited by moisture availability (Fig. 2). This is reflected in the PCA outcome, where individual ACTI records for the sites contributed either highly positively ( $>0.45$ ) or negatively ( $<-0.45$ ) to the ACTI components (not shown). The relationship between site locations and their response to climate (temperature, precipitation, and pressure) is described in detail by Seim et al. (2016) for a smaller TRW network in midlatitude Asia. Site chronologies with no significant responses to our classified circulation patterns might be controlled by climate conditions outside our target season (e.g., spring or the entire growing season). However, the focus here is on the identification of tree-growth-relevant synoptic-scale circulation patterns during summer and its comparison to observations.

High growth rates in trees that strongly contribute to ACTI\_1 were associated with above-normal sea level pressure (SLP) anomalies over the western and northern

parts of the study area (Fig. 3a). At 200-hPa geopotential height, a tripole pattern emerged with a high pressure center over northwestern Russia, a low pressure center over central and midlatitude Asia, and a high pressure system over southern China (Figs. 3b,c). Since jet streams are important factors affecting synoptic-scale weather conditions in the midlatitudes (Bluestein 1992; Holton and Hakim 2012), we computed spatial field correlation maps for 200-hPa zonal wind. Along the northern edge of the Tibetan Plateau, the subtropical jet stream strengthens, and anomalous cyclonic conditions prevail around Lake Balkhash (Kazakhstan in central Asia), causing higher-than-normal rainfall amounts and enhanced tree growth (Fig. 3e and Fig. S2e in the supplemental material). Conversely, the strong negative correlations for 200-hPa zonal wind indicates that enhanced westerlies, extending from the Mediterranean region to midlatitude Asia (Fig. 3c), cause dry climate conditions and thus, growth-limiting conditions in central and midlatitude Asia (Fig. 3d). The second ACTI mode, ACTI\_2, showed similar spatial correlation patterns to ACTI\_1, but with more westward displaced pressure centers (Figs. 3a–c,f–h), resulting in similar, but slightly displaced, temperature and precipitation response patterns (Figs. 3i,j) as for ACTI\_1.

Interestingly, the SLP and temperature patterns associated with ACTI\_1 and ACTI\_2 highly resemble those associated with Eurasian summer heat waves of continental scale, as was found during the Russian heat wave in 2010 by Dole et al. (2011). Schubert et al. (2014) performed a rotated empirical orthogonal function (REOF) analysis on summer temperature and precipitation over northern Eurasia and suggested prominent spatial patterns responsible for regional heat waves and droughts. The ACTI\_1 and ACTI\_2 patterns highly resemble the second and first REOF patterns, respectively, found by Schubert et al. (2014). Schubert et al. (2014) suggest that their REOF patterns represent stationary Rossby waves emanating from eastern Europe to northeastern Asia, contributing to the heat waves and droughts over northern Eurasia. Therefore, resulting temperature and precipitation changes could affect tree growth over the study area. Potential impacts of these large-scale atmospheric waves on moisture variability, as inferred from the ratio of stable oxygen isotopes in tree rings, were recently identified for the southeastern Tibetan Plateau (Wernicke et al. 2017b).

Different growth-circulation response patterns were obtained for the higher-order modes, ACTI\_3 and ACTI\_4. Sites assigned to ACTI\_3 were positively associated with SLP anomalies that extend diagonally from the Arabian Peninsula to northwestern Russia (Fig. 3k). At the 200-hPa level, a zonal structure with a

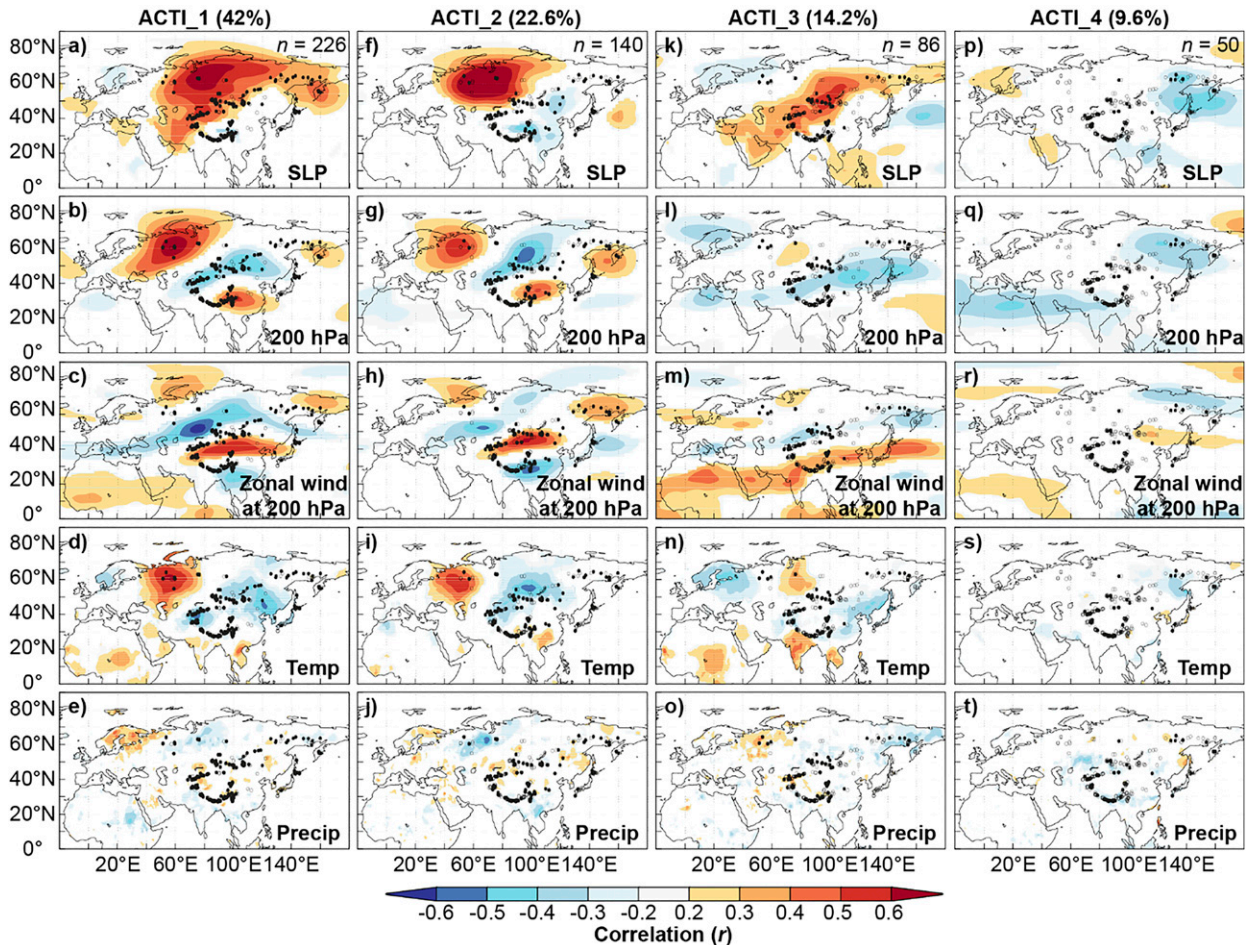


FIG. 3. Spatial field correlations of (left)–(right) the four ACTI components (ACTI\_1–ACTI\_4) and JJA mean SLP, pressure anomalies and zonal wind at 200-hPa geopotential height from the NOAA–CIRES twentieth-century reanalysis dataset, and temperature and precipitation from the CRU TS3.23 dataset for the period 1901–2010. Data were high-pass filtered (year-to-year difference). Black dots represent sites  $n$  with factor loadings on the principal components exceeding  $\pm 0.45$ .

low pressure center over northeastern China was visible (Fig. 3l). This structure is accompanied by positive associations of a southward-shifted subtropical jet stream extending from the Sahara to the Middle East to East Asia (Fig. 3m). This synoptic-scale circulation constellation is associated with growth-limiting conditions in the midlatitudes but with favorable conditions in southern Asia (Fig. 3n). Enhanced tree growth at the sites contributing most to the ACTI\_4 mode is associated with below-normal SLP anomalies that originate from the northern and tropical Pacific (Fig. 3p). The most pronounced feature of ACTI\_4 is its negative association with 200-hPa pressure anomalies over northeastern Russia (Fig. 3q), influencing the climate in this area, as well as in northeastern China and the Korea Peninsula (Figs. 3s,t). Although not strong, the overall pattern is reminiscent of the primary mode of the East Asian summer monsoon (Lau et al. 2000).

### c. Tree rings versus climate-derived circulation patterns: A spatiotemporal comparison

The leading tree-growth-relevant circulation patterns, that is, the ACTI modes, were compared to leading modes derived from summer H500 fields (Fig. 4). The first four H500 modes together explain 66.2% of the total variance, and simple correlation statistics showed that the corresponding pressure patterns were captured by the first four ACTI modes, explaining approximately 88% of the total variance (Table 1 and Fig. 4). ACTI\_1 highly corresponded to H500\_2 ( $r = 0.67$ ;  $p < 0.001$ ), ACTI\_2 corresponded to H500\_3 ( $r = 0.63$ ;  $p < 0.001$ ), and ACTI\_3 corresponded to H500\_4 ( $r = 0.24$ ;  $p < 0.01$ ), whereas ACTI\_4 was negatively associated with H500\_3 ( $r = 0.18$ ;  $p < 0.05$ ). The first three ACTI modes show temporally stable associations to the leading H500 modes over the last century (Fig. 4, right). Although the

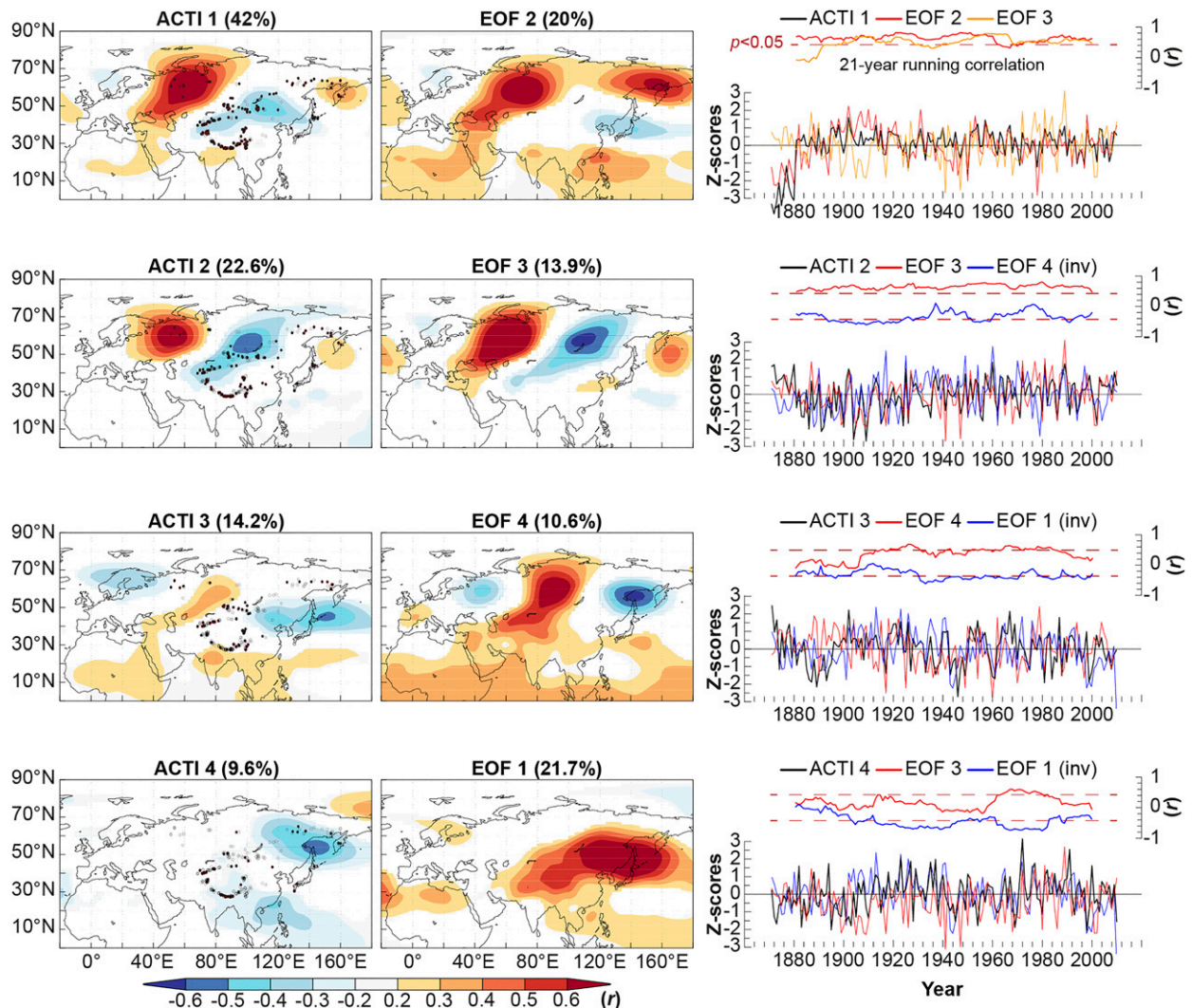


FIG. 4. Spatial field correlations of the (left) four leading ACTI modes and (center) corresponding H500 modes for pressure anomalies at 500-hPa geopotential height over the period 1901–2010. (right, top panels) Temporal relationships between the leading ACTI and H500 scores using 21-yr running correlations [Pearson correlation coefficients  $r$ ]. (right, bottom panels) Colors for the H500 scores (inv stands for inverted) correspond to the 21-yr running correlation (positive correlation values are shown in red and orange, and negative correlation values are in blue). Red dashed lines indicate the 95% significance level.

H500\_1 mode exhibited the highest amount of explained variance (21.7%), trees show a negative but significant association with this pressure pattern. This observation is especially evident for the ACTI\_3 and ACTI\_4 modes, which together contained 84% of the circulation variability of H500\_1 (Table 1). Interestingly, the other ACTI modes captured, to different extents, the leading circulation patterns. For instance, ACTI\_1, ACTI\_2, and ACTI\_3 almost fully represent the H500\_3 mode (Table 1).

It is important to note that the twentieth-century reanalysis data for the Asian continent are less reliable prior to 1900, and in some areas to 1950, because of

missing station data (Compo et al. 2011). Thus, higher uncertainties in the reanalysis dataset may introduce higher uncertainties in our results in the early parts of the analyzed period. For this reason, we tested the climate information extracted by the leading ACTI modes over the shorter 1950–2010 period (Fig. S2). Results obtained over the full and shorter periods are in agreement, whereas Schultz et al. (2015) found similar large-scale circulation patterns in their study of Europe by using a subjective weather-type classification. Moreover, our results indicate that tree growth in Asia is predominantly influenced by large-scale North Atlantic circulation patterns, which is in agreement with studies

TABLE 1. Pearson correlation coefficients between ACTI and H500 modes for the period 1871–2010. Correlation values exceeding the 95% (99%) significance level are indicated by one (two) asterisk(s).

	H500_1	H500_2	H500_3	H500_4
ACTI_1	−0.06	0.67**	0.19*	−0.11
ACTI_2	0.03	−0.11	0.63**	−0.34**
ACTI_3	−0.40**	0.21*	0.02	0.24*
ACTI_4	−0.44**	−0.07	0.18*	0.05

using climate data on shorter time scales (e.g., [Zhu et al. 2011](#)). This can be explained by the eastward propagation of the upper-tropospheric westerlies, manifested by the summer circumglobal wave train, which modulates local temperature and precipitation across Eurasia ([Ding and Wang 2005](#); [Saeed et al. 2014](#); [Zhu et al. 2011](#)), and in monsoon Asia (e.g., [Wernicke et al. 2017a,b](#)), which is linked to the Indian summer monsoon and ENSO ([Ding and Wang 2005](#)).

Our study was based on TRW chronologies with preserved interannual to decadal variability, and results provide valuable insights into the geographical extent of atmospheric circulation patterns at short to decadal time scales over Eurasia. However, tree rings also exhibit low-frequency variations of multidecadal-to-centennial time scale. Thus, tree-ring-based field reconstructions of climate [e.g., by using the nested point-by-point regression method; e.g., [Cook et al. \(2010\)](#)] and for different frequency domains will allow for an improved understanding of the magnitude and duration of past climate variability and its underlying circulation dynamics. This is demonstrated in [Luterbacher et al. \(2002\)](#) for the North Atlantic–European region using documentary evidences. Additionally, high-resolution field estimates of past climate will be useful to validate and improve model-generated products, which in turn will benefit more accurate climate predictions and climate change impact assessments.

#### 4. Conclusions

We applied the new ACTI method to a network of 414 TRW chronologies from Asia and extracted summer-time weather types relevant to tree growth. This allows us to assess synoptic-scale atmospheric circulation patterns and their impact on local and regional surface climate. By comparing synoptic patterns in the leading modes of the H500 anomalies, we find that the climate associated with pressure anomalies over northern Eurasia and midlatitude Asia had the most pronounced influence on the majority of trees in the region. Moreover, we show that the leading ACTI modes highly

correspond to the leading modes of H500 anomaly fields in space and time. Additionally, the observed significant statistical relationships between TRW and ACTI series, or rather weather types, allow us to reconstruct the ACTI time series. These reconstructed ACTI series, together with the weather-type weights, can be used to invert the model for periods without climate data and consequently lays the foundation to reconstruct pressure anomalies for different geopotential heights over Asia. This enables science to investigate climate and atmospheric circulation variability further back in time and validate and improve climate model simulations.

*Acknowledgments.* We are grateful to all colleagues who have provided tree-ring data to the International Tree-Ring Data Bank and to the anonymous reviewers for valuable comments on an earlier version of this manuscript. This research was supported by the Swedish International Development Cooperation Agency (SIDA; Project SWE-2009-245) and contributes to the strategic research areas Modelling the Regional and Global Earth System (MERGE), and Biodiversity and Ecosystem Services in a Changing Climate (BECC). This is Contribution No. 36 from the Sino-Swedish Centre for Tree-Ring Research (SISTR). H. W. Linderholm was financially supported by the Swedish Research Council (VR; Grants 2012-5246 and 2015-04031), E. Liang was supported by the National Natural Science Foundation of China (41525001), and J.-H. Jeong was supported by the National Research Foundation of Korea (2016R1A6A1A03012647).

#### REFERENCES

- Ahmed, M., and Coauthors, 2013: Continental-scale temperature variability during the past two millennia. *Nat. Geosci.*, **6**, 339–346, <https://doi.org/10.1038/ngeo1797>.
- Barry, R. G., and A. H. Perry, 1973: *Synoptic Climatology: Methods and Applications*. Methuen, 555 pp.
- Bluestein, H. B., 1992: *Synoptic-Dynamic Meteorology in Mid-latitudes: Observations and Theory of Weather Systems*. Oxford University Press, 448 pp.
- Carvajal-Rodríguez, A., J. de Uña-Alvarez, and E. Rolán-Alvarez, 2009: A new multitest correction (SGoF) that increases its statistical power when increasing the number of tests. *BMC Bioinf.*, **10**, 209, <https://doi.org/10.1186/1471-2105-10-209>.
- Chen, F., and Coauthors, 2008: Holocene moisture evolution in arid central Asia and its out-of-phase relationship with Asian monsoon history. *Quat. Sci. Rev.*, **27**, 351–364, <https://doi.org/10.1016/j.quascirev.2007.10.017>.
- Compo, G. P., and Coauthors, 2011: The Twentieth Century Reanalysis Project. *Quart. J. Roy. Meteor. Soc.*, **137**, 1–28, <https://doi.org/10.1002/qj.776>.
- Cook, E. R., and K. Peters, 1981: The smoothing spline: A new approach to standardizing forest interior tree-ring width series for dendroclimatic studies. *Tree-Ring Bull.*, **41**, 45–53.

- , and —, 1997: Calculating unbiased tree-ring indices for the study of climatic and environmental change. *Holocene*, **7**, 361–370, <https://doi.org/10.1177/095968369700700314>.
- , K. Anchukaitis, B. Buckley, R. D'Arrigo, G. Jacoby, and W. Wright, 2010: Asian monsoon failure and megadrought during the last millennium. *Science*, **328**, 486–489, <https://doi.org/10.1126/science.1185188>.
- Coumou, D., and S. Rahmstorf, 2012: A decade of weather extremes. *Nat. Climate Change*, **2**, 491–496, <https://doi.org/10.1038/nclimate1452>.
- Dando, W. A., 2005: Asia, climates of Siberia, central and East Asia. *Encyclopedia of World Climatology*, J. E. Oliver, Ed., Springer, 102–114, [https://doi.org/10.1007/1-4020-3266-8\\_19](https://doi.org/10.1007/1-4020-3266-8_19).
- Davi, N. K., R. D'Arrigo, G. Jacoby, E. Cook, K. Anchukaitis, B. Nachin, M. Rao, and C. Leland, 2015: A long-term context (931–2005 C.E.) for rapid warming over central Asia. *Quat. Sci. Rev.*, **121**, 89–97, <https://doi.org/10.1016/j.quascirev.2015.05.020>.
- Ding, Q., and B. Wang, 2005: Circumglobal teleconnection in the Northern Hemisphere summer. *J. Climate*, **18**, 3483–3505, <https://doi.org/10.1175/JCLI3473.1>.
- Dole, R., and Coauthors, 2011: Was there a basis for anticipating the 2010 Russian heat wave? *Geophys. Res. Lett.*, **38**, L06702, <https://doi.org/10.1029/2010GL046582>.
- Enke, W., and A. Spekat, 1997: Downscaling climate model outputs into local and regional weather elements by classification and regression. *Climate Res.*, **8**, 195–207, <https://doi.org/10.3354/cr008195>.
- Fang, K., N. Davi, X. Gou, F. Chen, E. Cook, J. Li, and R. D'Arrigo, 2010: Spatial drought reconstructions for central high Asia based on tree rings. *Climate Dyn.*, **35**, 941–951, <https://doi.org/10.1007/s00382-009-0739-9>.
- Fritts, H., 1976: *Tree Rings and Climate*. Academic Press, 567 pp.
- Hansen, G., and W. Cramer, 2015: Global distribution of observed climate change impacts. *Nat. Climate Change*, **5**, 182–185, <https://doi.org/10.1038/nclimate2529>.
- Holton, J. R., and G. J. Hakim, 2012: *An Introduction to Dynamic Meteorology*. 5th ed. International Geophysics Series, Vol. 88, Academic Press, 552 pp.
- IPCC, 2013: *Climate Change 2013: The Physical Science Basis*. Cambridge University Press, 1535 pp., <https://doi.org/10.1017/CBO9781107415324>.
- Krusic, P. J., E. Cook, D. Dukpa, A. Putnam, S. Rupper, and J. Schaefer, 2015: Six hundred thirty-eight years of summer temperature variability over the Bhutanese Himalaya. *Geophys. Res. Lett.*, **42**, 2988–2994, <https://doi.org/10.1002/2015GL063566>.
- Lau, K., K. Kim, and S. Yang, 2000: Dynamical and boundary forcing characteristics of regional components of the Asian summer monsoon. *J. Climate*, **13**, 2461–2482, [https://doi.org/10.1175/1520-0442\(2000\)013<2461:DABFCO>2.0.CO;2](https://doi.org/10.1175/1520-0442(2000)013<2461:DABFCO>2.0.CO;2).
- Li, J., and Coauthors, 2013: El Niño modulations over the past seven centuries. *Nat. Climate Change*, **3**, 822–826, <https://doi.org/10.1038/nclimate1936>.
- Liang, E., X. Shao, and N. Qin, 2008: Tree-ring based summer temperature reconstruction for the source region of the Yangtze River on the Tibetan Plateau. *Global Planet. Change*, **61**, 313–320, <https://doi.org/10.1016/j.gloplacha.2007.10.008>.
- Linderholm, H. W., C. K. Folland, and A. Walther, 2009: A multi-century perspective on the summer North Atlantic Oscillation (SNAO) and drought in the eastern Atlantic Region. *J. Quat. Sci.*, **24**, 415–425, <https://doi.org/10.1002/jqs.1261>.
- Luterbacher, J., and Coauthors, 2002: Reconstruction of sea level pressure fields over the eastern North Atlantic and Europe back to 1500. *Climate Dyn.*, **18**, 545–561, <https://doi.org/10.1007/s00382-001-0196-6>.
- Michaelsen, J., 1989: Long-period fluctuations in El Niño amplitude and frequency reconstructed from tree-rings. *Aspects of Climate Variability in the Pacific and the Western Americas*, *Geophys. Monogr.*, Vol. 55, Amer. Geophys. Union, 69–74.
- Mirza, M. M. Q., 2011: Climate change, flooding in South Asia and implications. *Reg. Environ. Change*, **11**, 95–107, <https://doi.org/10.1007/s10113-010-0184-7>.
- Osborn, T., K. Briffa, and P. Jones, 1997: Adjusting variance for sample-size in tree-ring chronologies and other regional mean timeseries. *Dendrochronologia*, **15**, 89–99.
- Peters, K., G. C. Jacoby, and E. R. Cook, 1981: Principal components analysis of tree-ring sites. *Tree-Ring Bull.*, **41**, 1–19.
- Philipp, A., C. Beck, R. Huth, and J. Jacobeit, 2016: Development and comparison of circulation type classifications using the COST 733 dataset and software. *Int. J. Climatol.*, **36**, 2673–2691, <https://doi.org/10.1002/joc.3920>.
- Rao, M. P., and Coauthors, 2015: Dzuds, droughts, and livestock mortality in Mongolia. *Environ. Res. Lett.*, **10**, 074012, <https://doi.org/10.1088/1748-9326/10/7/074012>.
- Saeed, S., N. Van Lipzig, W. A. Müller, F. Saeed, and D. Zanchettin, 2014: Influence of the circumglobal wave-train on European summer precipitation. *Climate Dyn.*, **43**, 503–515, <https://doi.org/10.1007/s00382-013-1871-0>.
- Sano, M., P. Tshering, J. Komori, K. Fujita, C. Xu, and T. Nakatsuka, 2013: May–September precipitation in the Bhutan Himalaya since 1743 as reconstructed from tree ring cellulose  $\delta^{18}\text{O}$ . *J. Geophys. Res. Atmos.*, **118**, 8399–8410, <https://doi.org/10.1002/jgrd.50664>.
- Schubert, S. D., H. Wang, R. D. Koster, M. J. Suarez, and P. Ya. Groisman, 2014: Northern Eurasian heat waves and droughts. *J. Climate*, **27**, 3169–3207, <https://doi.org/10.1175/JCLI-D-13-00360.1>.
- Schultz, J. A., and B. Neuwirth, 2012: A new atmospheric circulation tree-ring index (ACTI) derived from climate proxies: Procedure, results and applications. *Agric. For. Meteorol.*, **164**, 149–160, <https://doi.org/10.1016/j.agrformet.2012.05.007>.
- , C. Beck, G. Menz, B. Neuwirth, C. Ohlwein, and A. Philipp, 2015: Sensitivity of proxies on non-linear interactions in the climate system. *Sci. Rep.*, **5**, 18560, <https://doi.org/10.1038/srep18560>.
- Seim, A., and Coauthors, 2016: Synoptic-scale circulation patterns during summer derived from tree rings in mid-latitude Asia. *Climate Dyn.*, **49**, 1917–1931, <https://doi.org/10.1007/s00382-016-3426-7>.
- Shepherd, T. G., 2014: Atmospheric circulation as a source of uncertainty in climate change projections. *Nat. Geosci.*, **7**, 703–708, <https://doi.org/10.1038/ngeo2253>.
- Shi, F., and Coauthors, 2015: A multi-proxy reconstruction of spatial and temporal variations in Asian summer temperatures over the last millennium. *Climatic Change*, **131**, 663–676, <https://doi.org/10.1007/s10584-015-1413-3>.
- Solomina, O., O. Maximova, and E. Cook, 2014: *Picea schrenkiana* ring width and density at the upper and lower tree limits in the Tien Shan Mts (Kyrgyz Republic) as a source of paleoclimatic information. *Geogr., Environ., Sustain.*, **7**, 66–79, <https://doi.org/10.24057/2071-9388-2014-7-1-66-79>.
- van Oldenborgh, G. J., and G. Burgers, 2005: Searching for decadal variations in ENSO precipitation teleconnections. *Geophys. Res. Lett.*, **32**, L15701, <https://doi.org/10.1029/2005GL023110>.
- Wernicke, J., P. Hochreuther, J. Griebinger, H. Zhu, L. Wang, and A. Bräuning, 2017a: Air mass origin signals in  $\delta^{18}\text{O}$

- of tree-ring cellulose revealed by back-trajectory modeling at the monsoonal Tibetan plateau. *Int. J. Biometeor.*, **61**, 1109–1124, <https://doi.org/10.1007/s00484-016-1292-y>.
- , —, —, —, —, and —, 2017b: Multi-century humidity reconstructions from the southeastern Tibetan Plateau inferred from tree-ring  $\delta^{18}\text{O}$ . *Global Planet. Change*, **149**, 26–35, <https://doi.org/10.1016/j.gloplacha.2016.12.013>.
- Wigley, T. M., K. R. Briffa, and P. D. Jones, 1984: On the average value of correlated time series, with applications in dendroclimatology and hydrometeorology. *J. Climate Appl. Meteor.*, **23**, 201–213, [https://doi.org/10.1175/1520-0450\(1984\)023<0201:OTAVOC>2.0.CO;2](https://doi.org/10.1175/1520-0450(1984)023<0201:OTAVOC>2.0.CO;2).
- Yadav, R. R., A. Braeuning, and J. Singh, 2011: Tree ring inferred summer temperature variations over the last millennium in western Himalaya, India. *Climate Dyn.*, **36**, 1545–1554, <https://doi.org/10.1007/s00382-009-0719-0>.
- Yancheva, G., and Coauthors, 2007: Influence of the intertropical convergence zone on the East Asian monsoon. *Nature*, **445**, 74–77, <https://doi.org/10.1038/nature05431>.
- Zhu, X., O. Bothe, and K. Fraedrich, 2011: Summer atmospheric bridging between Europe and East Asia: Influences on drought and wetness on the Tibetan Plateau. *Quat. Int.*, **236**, 151–157, <https://doi.org/10.1016/j.quaint.2010.06.015>.